Secure Systems Design and Technology Development. Veliko Tarnovo, Bulgaria
Proceedings of the International Scientific Conference, 2026. Volume II, 465-473

Influence of Pass Configuration, Raster Step, and Scanning Speed on Laser Color Marking of AISI 304 Steel

Lyubomir Lazov
Rezekne Academy of Riga Technical University
Rezekne, Latvia
lyubomir.lazov@rtu.lv

Nikolay Angelov
Rezekne Academy of Riga Technical University
Rezekne, Latvia
angelov_np@abv.bg

Erika Teirumnieka
Rezekne Academy of Riga Technical University
Rezekne, Latvia
erika.teirumnieka@rtu.lv

***Abstract*—Experiments were carried out on the process of color marking with a fiber laser on AISI 304 steel samples. The influence of the number of passes - one (at 0°), two (at 0° and 90°) and three (at 0°, 60° and 120°), the raster step and the scanning speed on the roughness and the resulting colors was studied. R/G/B coordinates of all marked squares were obtained. The positions of the individual colors in the color space were determined. Graphs of the dependence of the roughness on the raster step were constructed for three speeds and for the three types of passes. The obtained results were analyzed and summarized.**

Keywords— lase rmarking, steel AISI 304, raster step, speed, color difference, chromatic distance.

I. Introduction

Laser marking has become a widely adopted technology in modern manufacturing due to its high precision, flexibility, and non-contact nature [1] – [8]. Among the various laser-based surface processing techniques, color laser marking has gained significant attention, particularly for stainless steels, where it enables the generation of stable and reproducible colors without the use of pigments or coatings. This process relies on the controlled formation of thin oxide layers on the material surface, which produce colors through light interference effects.

AISI 304 stainless steel is one of the most commonly used austenitic steels due to its excellent corrosion resistance, mechanical properties, and wide applicability in industries such as food processing, medical equipment, construction, and consumer goods. The ability to perform color marking on this material expands its functional and aesthetic applications, including product identification, anti-counterfeiting, branding, and decorative design.

The quality and characteristics of laser-induced colors strongly depend on process parameters such as laser power, pulse duration, scanning speed, raster step, and scanning strategy. These parameters determine the thermal input, oxidation kinetics, and surface morphology, which in turn influence both the optical properties and the roughness of the treated surface. In particular, raster-based marking strategies and multi-pass configurations introduce complex interactions between overlapping laser tracks, affecting energy distribution and heat accumulation [9] – [17].

Previous studies have shown that surface roughness plays a crucial role in color formation, as it affects light scattering and interference conditions. At the same time, scanning speed and raster step control the energy density delivered to the material, thereby influencing oxide layer thickness and uniformity [18] – [24]. However, the combined effect of these parameters, especially when different pass configurations are applied, remains insufficiently explored.

The present study aims to investigate the influence of raster step, scanning speed, and pass configuration (single-, double-, and triple-angle marking) on the surface roughness and color characteristics of AISI 304 stainless steel during fiber laser marking. By systematically analyzing these parameters and correlating them with RGB (red, green, blue) color data and surface measurements, the work seeks to provide a deeper understanding of the mechanisms governing laser color marking and to identify optimal processing conditions for achieving high-quality and reproducible results. 08X18H10

Online ISSN 3044-7771
https://doi.org/10.68302/std2026.vol2.209

II. Materials and Methods

A. Material

AISI 304 stainless steel is one of the most widely used stainless steels. Нейните основни индустриални приложения са in the food-beverage industry (processing equipment, storage tanks, kitchen appliances), the construction and architecture (structural components, railings, decorative finishes), the chemical industry (piping systems, heat exchangers, storage vessels for chemicals), the medical and pharmaceutical products (surgical instruments, sterile processing systems), automotive industry (exhaust components, structural parts) and consumer products (sinks, cookware, cutlery, washing machines, water heaters).

The chemical composition of AISI 304 steel is given in Table 1. This composition is carefully balanced to ensure an optimal combination of corrosion resistance, workability, and cost.

Alloying elements influence the steel's internal structure. Carbon influences strength, hardness and ductility and weldability. It is low carbon steel and is soft, ductile and easy to weld. The high chromium content improves the corrosion resistance of this steel by making it stainless (a passive oxide layer is formed by passivation). Nickel increases its toughness and stabilizes the austenite phase.

TABLE 1 CHEMICAL COMPOSITION OF AISI 304 STEEL

Element	Content, %	Element	Content, %
C	< 0.08	Ni	8.0 – 10.5
Cr	18.0 – 20.0	Mg	< 2.0
Si	< 1.0	P	< 0.045
S	< 0,03	Fe	Balance

Some physical properties of the steel are presented in Table 2. This steel has a density typical of steels and a relatively high specific heat capacity, which requires more energy to heat than low-alloy steels. Thermal conductivity is moderate, the coke is typical of stainless steels, which are not good heat conductors. It has a relatively low thermal diffusivity, as heat spreads slowly inside the material and the surface heats up faster.

TABLE 2 BASIC OPTICAL AND THERMOPHYSICAL PARAMETERS OF AISI 304 STEEL

Parameter	Value
Coefficient of thermal conductivity k, W/(m·K)	17
Density ρ, kg/m^3	7850
Specific heat capacity c, J/(kg·K)	504
Coefficient of thermal diffusivity a, m^2/s	4.3×10^{-6}

B. Laser system

A laser technological system equipped with a fiber laser Rofin PowerLine F20 Varia was used to conduct the experiments. The main technical parameters of both the laser system and the laser source are summarized in Table 3.

The laser operates in the near-infrared spectral range at a wavelength of 1064 nm, which is characteristic of ytterbium-doped fiber lasers and ensures good absorption in metallic materials such as stainless steels. The system functions in pulsed mode, allowing precise control over energy input and minimizing excessive thermal loading of the treated surface.

The laser source is distinguished by its excellent beam quality ($M^2 < 1.1$), which enables tight focusing of the beam to a small spot diameter of approximately 70 µm. This results in high power density and makes the system particularly suitable for localized surface treatment processes such as laser marking, hardening, micro-processing, and precision structuring.

Another important feature of the system is its wide operating frequency range (20–250 kHz), which allows flexibility in adjusting the interaction between the laser radiation and the material. The short pulse duration (100 ns) combined with adjustable pulse energy (0.08–1.00 mJ) and high peak power (up to 10 kW) ensures efficient energy delivery within a very short time interval. This promotes rapid heating and cooling cycles, which are essential for achieving controlled microstructural transformations without affecting the bulk material.

In addition, the laser system is characterized by high positioning accuracy (± 2.5 µm), enabling precise control of the processing path and repeatability of the results. The relatively high efficiency (approximately 40%) of the fiber laser contributes to reduced energy consumption and stable operation during extended experimental runs.

Overall, these characteristics make the laser system highly suitable for advanced material processing applications requiring precision, repeatability, and controlled thermal input, particularly in the treatment of stainless steels such as AISI 304.

TABLE 3 MAIN PARAMETERS OF THE LASER SYSTEM FOR MARKING WITH FIBER LASER

Parameter	Value
Wavelength λ, nm	1064
Power P, W	20
Frequency ν, kHz	20 – 250
Pulse duration τ, ns	100
Pulse energy E_p, mJ	0.08 – 1.00
Pulse power P_p, kW	0.80 - 10
Diameter in focus d, µm	70
Beam quality M^2	< 1.1
Positioning accuracy	± 2.5 µm

Efficiency, %	40

C. Methodology

The experimental study was carried out through a sequence of systematically organized stages aimed at evaluating the influence of key technological parameters – namely raster pitch and scanning speed – on the surface characteristics and color properties obtained during raster laser marking of AISI 304 stainless steel.

To investigate the effect of laser scanning strategies, three marking configurations were developed:

Single-angle marking (0°)

Double-angle marking (0° and 90°)

Triple-angle marking (0°, 60°, and 120°)

For each configuration, a matrix consisting of 3 rows and 8 columns (24 squares in total) was designed, as illustrated in Figure 1. Each square had dimension of 5 mm and was raster-marked under distinct processing conditions.

Within each matrix, the raster step (distance between adjacent scan lines) was varied in the range 20 µm to 80 µm. The scanning speed was varied from 25 mm/s to 125 mm/s, with increments of 50 mm/s.

The preparation of the test specimens was the next step to ensure repeatability and reliability of results. The procedure included:

- Cutting the AISI 304 stainless steel samples to the required dimensions

- Surface grinding and polishing to obtain a uniform initial roughness

- Cleaning the surfaces to remove contaminants that could affect laser-material interaction

Proper surface preparation ensured that any observed changes in roughness and color were solely due to the laser processing parameters.

The experiments were conducted using a fiber laser system (Rofin PowerLine F20 Varia), operating in pulsed mode in the near-infrared range (λ = 1064 nm).

Raster marking was performed by scanning the laser beam line-by-line over each square area. The variation of raster pitch and scanning speed directly influenced energy input per unit area and overlap between successive laser tracks. These factors are essential in determining the formation of oxide layers responsible for color generation on stainless steel surfaces.

Surface roughness was measured using a laser scanning microscope OLS5100, which provides high-resolution, non-contact surface profiling. The roughness analysis allowed assessment of surface morphology changes and correlation between processing parameters and surface texture

The color of each marked square was recorded and expressed in terms of RGB (Red, Green, Blue) coordinates, which represent the digital color space.

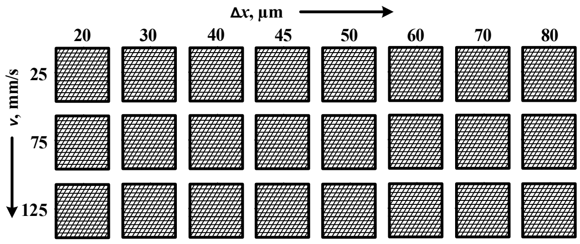

Fig. 1. Scheme of the matrix for conducting experiments on laser color marking

III. Results and discussion

After conducting the experiments and the necessary measurements, the influence of the raster pitch on the surface roughness of single-angle, double-angle and triple-angle marking and comparative analysis for a scanning speed of 125 mm/s was analysed. The raster pitch varies in the range from 20 µm to 80 µm, and three marking speeds were studied: 25 mm/s, 75 mm/s and 125 mm/s. The roughness of the untreated surface is R_a = 0.223 µm.

A. Influence of raster step on roughness

- Single-angle marking (0°)

The graphs of the dependence of the surface roughness on the raster step for three scanning speeds 25 mm/s, 75 mm/s and 125 mm/s are presented in Fig. 2. From their analysis, the following findings can be made:

- With increasing the raster step, a nonlinear increase in surface roughness is observed for the three studied speeds, which indicates that the spatial distribution of laser energy plays an important role in the formation of surface morphology;

- In the raster step interval from 20 µm to 50 µm, the rate of increase in roughness is greater compared to that in the interval from 50 µm to 80 µm. This behavior is explained by the scanning overlap coefficient. In the first interval, the overlap is larger, the absorbed energy is greater and surface melting occurs. In the second interval, the overlap is significantly smaller, reducing the absorbed energy compared to the first interval, which leads to a slower increase in roughness;

- At a speed of 25 mm/s, the roughness increases from 0.49 µm to 0.62 µm. At a speed of 75 mm/s, the roughness changes from 0.43 µm to 0.56 µm. At 125 mm/s, Ra increases from 0.38 µm to 0.53 µm.

- It is indirectly obtained that with increasing speed, a decrease in roughness is observed. Moreover, at the same raster steps, the roughness at 25 mm/s is about 13% higher than at 75 mm/s and 30% higher than at 125 mm/s. It is explained by stronger thermal effects at lower scanning speeds.

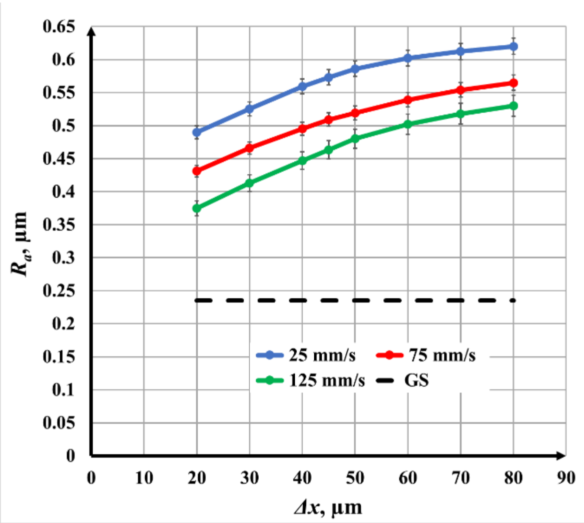

Figure 2. Graphs of roughness versus raster step for single-angle marking for three scanning speeds: blue color — 25 mm/s; orange color — 75 mm/s, and green color — 125 mm/s. The black dashed line is the roughness of the untreated surface.

- Double-angle marking (0° and 90°)

The graphs of the dependence of roughness on the raster pitch for double-angle marking are presented in Figure 3. From their analysis, the following conclusions can be drawn:

- The same trends are observed as for single-angle marking – a nonlinear increase in roughness with increasing raster step for the three studied speeds, the curves in the interval from 20 µm to 50 µm are steeper than from 50 µm to 80 µm;

- At a speed of 25 mm/s, the roughness increases from 0.41 µm to 0.54 µm. At a speed of 75 mm/s, the roughness varies from 0.34 µm to 0.49 µm. At a speed of 125 mm/s, the roughness changes from 0.29 µm to 0.45 µm;

- With increasing speed, a decrease in roughness is again observed. At a given raster step, the roughness at 25 mm/s is approximately 18% higher than at 75 mm/s and 37% higher than at 125 mm/s.

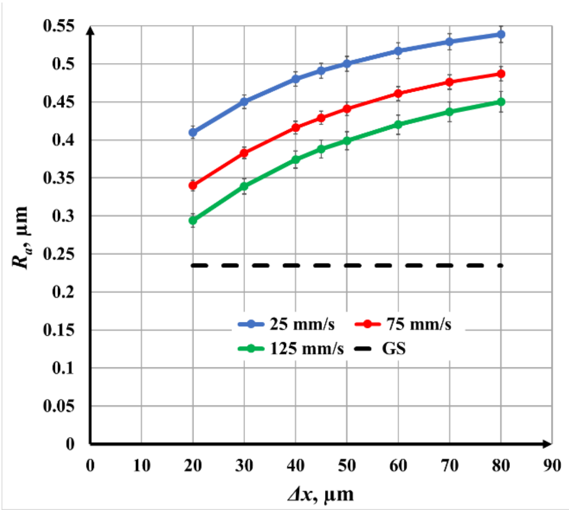

Figure 3. Graphs of roughness versus screen pitch for double-angle marking for three speeds: blue — 25 mm/s; orange — 75 mm/s and green — 125 mm/s. The black dashed line is the roughness of the unprocessed surface.

- Triple-angle marking (0°, 60° and 120°)

The graphs of the dependence of roughness on the raster pitch for triangular marking are given in Figure 4. From their analysis it follows:

- With increasing raster step, a nonlinear increase in roughness occurs. In the interval from 20 µm to 50 µm, the rate of increase in roughness is greater than that in the interval from 50 µm to 80 µm;

- At a speed of 25 mm/s, the roughness increases from µm 0.34 to 0.46µm for the studied interval of the raster step. At a speed of 75 mm/s, the roughness varies from 0.29 µm to 0.41 µm. At a speed of 125 mm/s, the roughness varies from 0.25 µm to 0.37 µm;

- At equal raster steps, the roughness at 25 mm/s is approximately 15% higher than at 75 mm/s and 35% higher than at 125 mm/s.

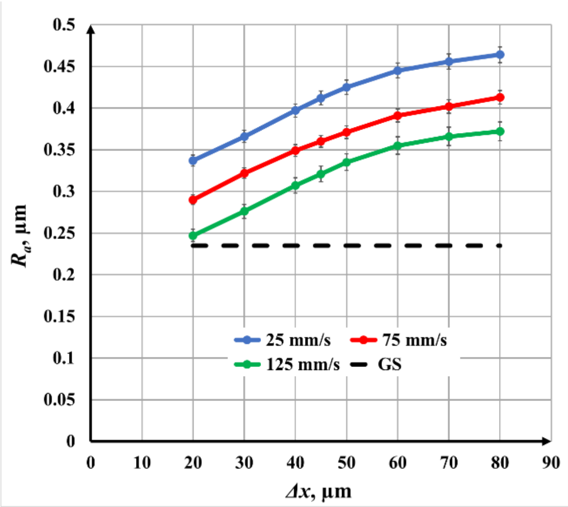

Figure 4. Graphs of the dependence of roughness on the raster step in triple-angle marking for three speeds: blue color — 25 mm/s; orange color — 75 mm/s and green color — 125 mm/s. The black dotted line is the roughness of the untreated surface.

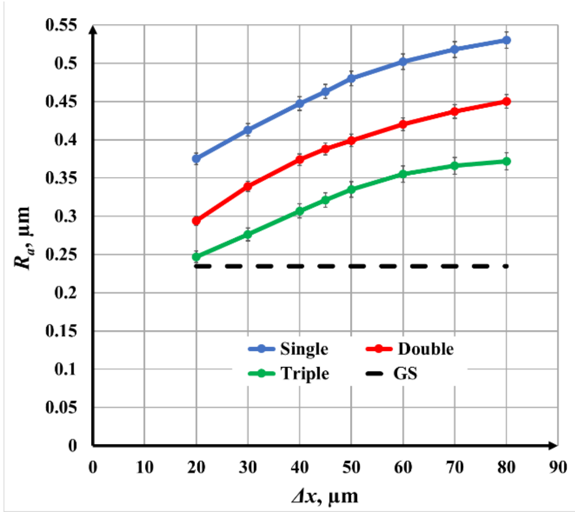

Figure 5. Graphics of the dependence of roughness on the raster step for speeds v = 125 mm/s: blue color – single-angle marking; red color – double-angle marking and green color – triple-angle marking. The black dotted line is the roughness of the unprocessed surface.

- Comparative analysis at 125 mm/s for roughness

A comparison of single-angle, double-angle and triple-angle marking at 125 mm/s is given in Figure 5. For all scanning strategies, increasing the raster step leads to a nonlinear increase in roughness. Their roughness values differ significantly. The highest roughness is observed for single-angle marking. The roughness for double-angle marking decreases by about 18%. The reduction in roughness compared with single-angle repetition is attributed to the cross-scanning strategy, which redistributes material and partially smooths anisotropic surface characteristics. Triple-angle marking has about 32% less roughness than single-angle marking. This comparison shows that the scanning strategy has as much of a role and influence in controlling surface roughness as the raster step and scanning speed. Multidirectional scanning not only changes the surface morphology but also improves the uniformity of the marking, which is critical for stable and reproducible color generation.

B. Influence of raster step on color

The color characteristics R/G/B for single-angle (0°), double-angle (0° and 90°) and triple-angle marking (0°, 60° and 120°) are summarized in Table 4, where each marked square is identified by its scanning speed and raster-step position - Table 4a for single-angle marking, Table 4b for double-angle marking and Table 4c for triple-angle marking. After using specialized software, the positions of the points in the color diagram that correspond to a specific color for each individual marked square were determined. In addition, all obtained RGB coordinates were converted to L*a*b*. Most of the obtained colors fall within the yellow spectral region, with noticeable variations in saturation.

TABLE 4 MAIN PARAMETERS OF THE LASER SYSTEM FOR MARKING WITH FIBER LASER

Δx, µm *v*, mm/s	20	30	40	45	50	60	70	80
25	1.1.1 12/0/136	1.1.2 15/36/130	1.1.3 13/135/63	1.1.4 13/135/53	1.1.5 65/140/52	1.1.6 155/230/150	1.1.7 255/255/182	1.1.8 255/255/185
75	1.3.1 255/255/90	1.3.2 255/255/144	1.3.3 255/255/173	1.3.4 255/255/183	1.3.5 255/255/195	1.3.6 255/255/205	1.3.7 255/255/212	1.3.8 255/255/219
125	1.5.1 255/255/102	1.5.2 255/255/156	1.5.3 255/255/186	1.5.4 255/255/200	1.5.5 255/255/210	1.5.6 255/255/221	1.5.7 255/255/232	1.5.8 255/255/245

a)

b)

Δx, µm *v*, mm/s	20	30	40	45	50	60	70	80
25	2.1.1 0/0/151	2.1.2 0/36/145	2.1.3 0/135/29	2.1.4 0/135/42	2.1.5 50/145/57	2.1.6 140/230/145	2.1.7 255/255/166	2.1.8 255/255/170
75	2.3.1 255/255/75	2.3.2 255/255/129	2.3.3 255/255/158	2.3.4 255/255/169	2.3.5 255/255/180	2.3.6 255/255/190	2.3.7 255/255/197	2.3.8 255/255/204
125	2.5.1 255/255/87	2.5.2 255/255/141	2.5.3 255/255/171	2.5.4 255/255/185	2.5.5 255/255/195	2.5.6 255/255/206	2.5.7 255/255/217	2.5.8 255/255/230

c)

Δx, µm *v*, mm/s	20	30	40	45	50	60	70	80
25	3.1.1 0/0/166	3.1.2 0/36/160	3.1.3 0/135/15	3.1.4 0/135/31	3.1.5 50/155/55	3.1.6 140/230/170	3.1.7 255/255/153	3.1.8 255/255/157
75	3.3.1 255/255/60	3.3.2 255/255/114	3.3.3 255/255/143	3.3.4 255/255/154	3.3.5 255/255/165	3.3.6 255/255/175	3.3.7 255/255/182	3.3.8 255/255/189
125	3.5.1 255/255/72	3.5.2 255/255/126	3.5.3 255/255/156	3.5.4 255/255/170	3.5.5 255/255/180	3.5.6 255/255/191	3.5.7 255/255/202	3.5.8 255/255/215

- Single-angle marking (0°)

Figure 6a shows the color diagram for 25 mm/s for single-angle marking. At small raster steps (20–30 µm), low speed and small raster steps corresponding to large coverage lead to high energy absorption, melting in the impact zone and the formation of darker colors, including violet-blue tones. With increasing raster step, the scanning overlap coefficient decreases and a transition from partial melting to oxidation occurs, corresponding to a transition through a green color with various shades to a yellow color.

Figure 6b shows the resulting color diagram for a scanning speed of 75 mm/s. Due to the significantly lower energy absorption at a speed of 25 mm/s, all marked areas remain in the yellow region. A decrease in their saturation with an increase in the raster step is observed, which is explained by the gradual formation of thinner oxide layers.

Figure 6c illustrates the results for a scanning speed of 125 mm/s. Again, yellow colors are obtained for the entire interval of the raster step and the trend of decreasing saturation with increasing raster step is maintained. Overall, the colors are less saturated than at 75 mm/s.

The analysis of the obtained results leads to the following generalizations for single-angle marking:

- With increasing roughness and raster step, a tendency for colors to move from darker to lighter or from more saturated to less saturated is observed;
- For a speed of 125 mm/s, the saturation of the obtained yellow colors is less than that for a speed of 75 mm/s for the entire studied interval of the raster step.

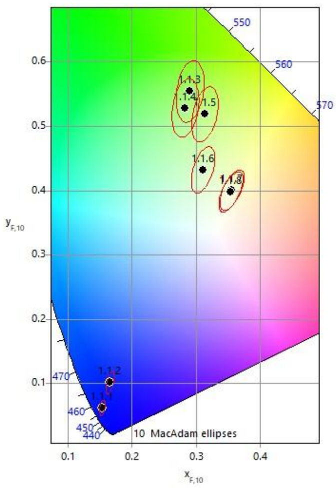

a)

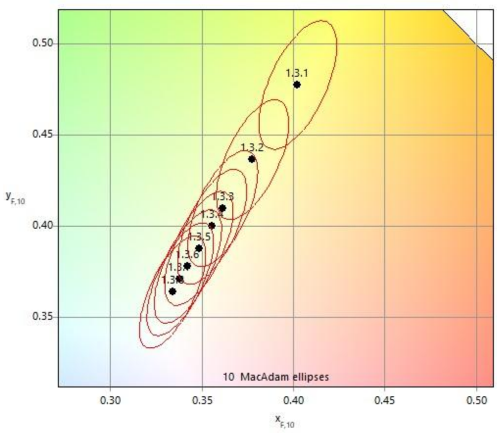

b)

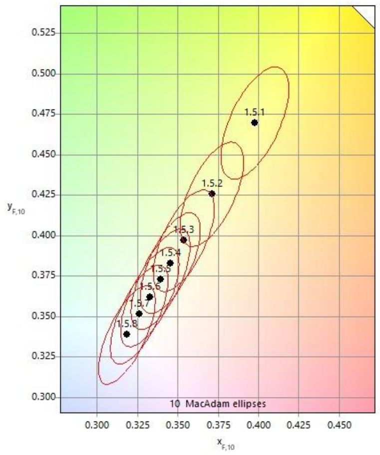

c)

Figure 6. Color diagram for single-angle marking for raster step in interval from 20 µm to 80 µm and speeds: a) 25 mm/s; b) 75 mm/s and c) 125 mm/s.

- Double-angle marking (0° and 90°)

Figure 7a shows the color diagram for 25 mm/s for double-angle marking. Again, the same trends are observed as with single-angle marking, namely:

- With increasing raster step, the colors transition from dark to lighter – from blue through green to yellow with different shades;
- For a certain raster step, the saturation of the corresponding color is greater than that when marking at an angle.

Figure 7b shows the color chart for 75 mm/s for double-angle marking. Again, the same trends are observed as for single-angle marking, namely:

- As the raster step increases, the colors go from dark to lighter - from blue to green to yellow with different shades;
- For a given raster step, the saturation of the corresponding color is less than that at a speed of 25 mm/s.

The color diagram for 125 mm/s is presented in Figure 7c. Again, similar findings can be made as for 25 mm/s and 75 mm/s:

- With increasing raster step, the colors go from dark to lighter - from blue through green to yellow with different shades;
- The difference from the previous two cases is that for the speed of 125 mm/s, the color saturation for the individual raster steps is the smallest.

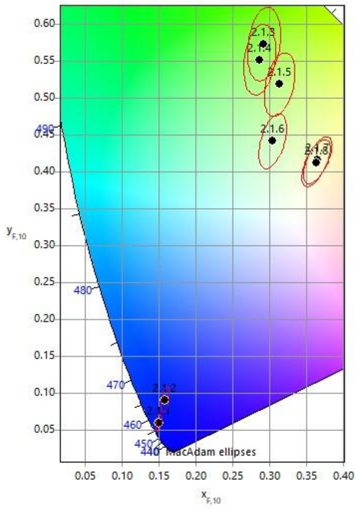

a)

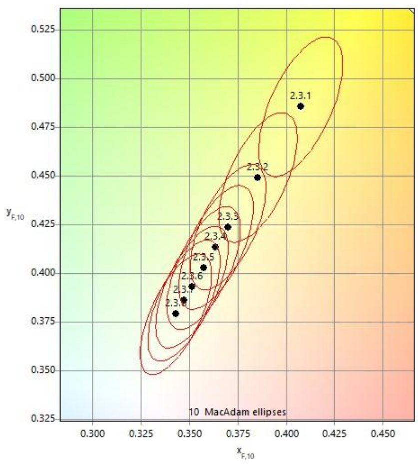

b)

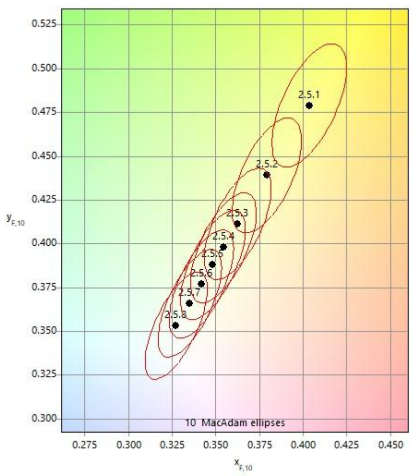

c)

Figure 7. Color diagram for double-angle marking for raster step in interval from 20 µm to 80 µm and speeds: a) 25 mm/s; b) 75 mm/s and c) 125 mm/s.

- Triple-angle marking

The color chart for 25 mm/s in triple-angle marking is presented in Figure 8a. The following trends are observed:

- With increasing raster step and roughness, the colors go from dark to lighter;
- For a given raster step, the saturation of the corresponding color is greater than that for single-angle and double-angle marking.

The color chart for 75 mm/s in triple-angle marking is given in Figure 8b. The following trends are observed:

- With increasing raster step, the colors go from dark to lighter - from blue to green to yellow with different shades;
- For a given raster step, the saturation of the corresponding color is less than that at 25 mm/s.

The color chart for 125 mm/s is given in Figure 8c. From their analysis, the following conclusions can be drawn:

- As the raster step increases, the colors go from dark to lighter;
- For a speed of 125 mm/s, the color saturation for the individual raster steps is the lowest.

The following main conclusions can be drawn for raster color marking of AISI 304 stainless steel samples:

- For single-angle, double-angle and triple-angle marking, with increasing raster step and roughness, either a transition from darker colors to lighter colors or from a more saturated yellow color to a less saturated color is observed;

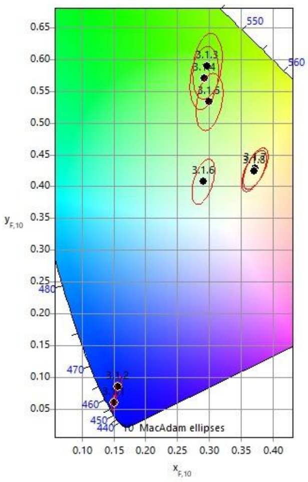

a)

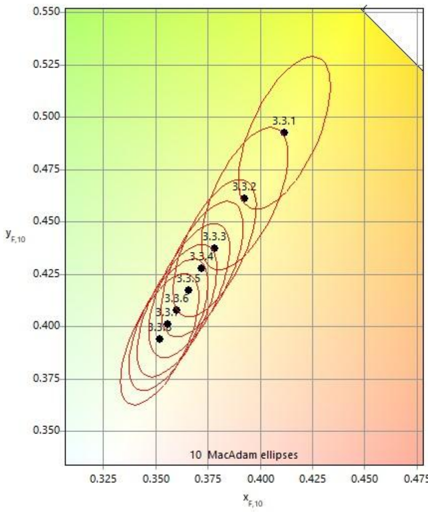

b)

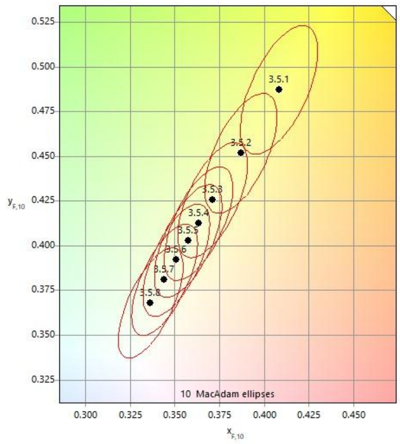

c)

Figure 8. Color diagram for double-angle marking for raster step in interval from 20 µm to 80 µm and speeds: a) 25 mm/s; b) 75 mm/s and c) 125 mm/s.

- With increasing speed, a decrease in color saturation is observed. Of the speeds studied, the least saturated colors are obtained at 125 mm/s;
- The most saturated colors are obtained with triple-angle marking, and the least saturated colors are obtained with single-angle marking.

IV. Conclusions

The present study investigates the influence of the raster pitch, scanning speed and pass configuration on the surface roughness and color characteristics obtained during laser marking of AISI 304 stainless steel.

Based on the experimental results obtained by the authors and their analysis, the following main conclusions can be drawn:

- Increasing the raster step leads to a nonlinear increase in surface roughness for all marking strategies. At the same time, it causes a transition from darker, more saturated colors to lighter, less saturated ones, due to the reduced energy load and the formation of a thinner oxide layer.
- Increasing the scanning speed leads to a decrease in surface roughness and color saturation. Higher speeds limit thermal build-up, which leads to thinner oxide layers and reduced intensity of the resulting colors.
- The scanning strategy has a significant influence on both roughness and color quality. Single-angle marking results in the highest roughness and least uniform colors. Double-angle marking improves uniformity and reduces roughness. Triple-angle marking provides the best results, with the lowest roughness and highest color saturation
- There is a strong relationship between surface morphology and optical properties. Lower roughness enhances light interference effects, resulting in more stable and saturated colors.

The results provide valuable guidance for industrial laser marking applications where precise color control and surface quality are required.

References

[1] J. Ion, Laser Processing of Engineering Materials, *Elsevier*, 2005, ps. 556, ISBN 978-0-7506-6079-2

[2] W. Steen, J. Mazumder Laser Material Processing, *Springer London*, 2010, ps. 558, https://doi.org/10.1007/978-1-84996-062-5

[3] N. Dahotre, S. Harimkar Laser Fabrication and Machining of Materials, *Springer New York*, 2008, ps. 558, https://doi.org/10.1007/978-0-387-72344-0

[4] J. Ready, Industrial Applications of Lasers, Elsevier, 1997, ps. 599, ISBN 9780080508603

[5] P. Gadhe, R. Bathe Laser Materials Processing for Industrial Applications, *Proceedings of the National Academy of Sciences, India - Section A*, 88(2), DOI: https://doi.org/10.1007/s40010-018-0523-5

[6] W. Khan, R. Yasmin Laser Technology: Bridging Historical Milestones and Modern Applications in Science, *Industry, and Sustainability, Global Scientific and Academic Research Journal of Multidisciplinary Studies*, 2025, pp. 70 – 84, DOI: https://doi.org/10.5281/zenodo.14770605

[7] M. Quazi Laser Technologies in Modern Materials Processing and Their Functional Applications, *Materials Research Express*, 12(8), 2025, DOI: https://doi.org/10.1088/2053-1591/adf494

[8] A. Temmler, D. Liu Influence of laser polishing on surface roughness and microstructural properties of the remelted surface boundary layer of tool steel H11, *Materials & Design*, Volume 192 108689, 2020, https://doi.org/10.1016/j.matdes.2020.108689

[9] E. Amara, F. Haïd, A. Noukaz Experimental Investigations on Fiber Laser Color Marking of Steels, *Applied Surface Science*, Volume 351, pp. 1-12, 2015, DOI: https://doi.org/10.1016/j.apsusc.2015.05.095

[10] J. Dowden The Theory of Laser Materials Processing, *Springer Dordrecht*, 2009, ps. 390, ISBN 978-1-4020-9340-1

[11] A. Schkutow, T. Frick Laser color marking of stainless steel – Investigation of the fluencedependent and thermal mechanisms in generating laser induced surface modifications, *Elsevier B.V. Procedia CIRP*, 124 661–664, 2024, DOI: https://doi.org/10.1016/j.procir.2024.08.196

[12] Y. Lu, X. Shi, Nanosecond Laser Coloration on Stainless Steel Surface, *Scientific Report*, 7: 7092, 2017, DOI: https://doi.org/10.1038/s41598-017-07373-8

[13] E. Pryakhin, A. Yu. Dranova, Application of direct laser marking of products made of different types of alloys using ultra-dense matrix nanobar-code, *CIS Iron and Steel Review*, Vol. 30, 2025, pp. 92–98, DOI: https://doi.org/10.17580/cisisr.2025.02.15

[14] N. Dolchinkov, T. Petrov Features of Color Laser Marking on Metals, *Environment. Technology. Resources. Proceedings of the 14th International Scientific and Practical Conference*, Volume 3, 297-305, https://doi.org/10.17770/etr2023vol3.7222

[15] M. Kucera, M.i Švanter, E. Smazalova Influence of Laser Marking on Stainless Steel Surface and Corrosion Resistance, *Metal 2014 Brno*, 2014, pp. 890 – 895

[16] N. Dolchinkov, Marking and Cutting of Non-metallic Products with CO2 Laser, IOP Publishing Ltd, Journal of Physics: Conference Series, Volume 2224, 2021 2nd International Symposium on Automation, Information and Computing (ISAIC 2021) 03/12/2021 - 06/12/2021 Online ISSN: 1742-6596, Print ISSN: 1742-6588, pp 1-8

[17] I.. Korolev, M. Kravchenko, E. Fedorova and N. Dolchinkov, Protection of biological objects from electromagnetic radiation, E3S Web of Conferences, 2023, 411, 02003, VI International Conference on Actual Problems of the Energy Complex and Environmental Protection (APEC-VI-2023), https://doi.org/10.1051/e3sconf/202341102003

[18] R. Linggamm, M. Quaz et al. Formation of Colours on SS304L Stainless Steel Induced by Laser Colouring, *IOP Conf. Series: Materials Science and Engineering*, 1078 012015, 2021, DOI: https://doi.org/10.1088/1757-899X/1078/1/012015

[19] M. Swayne, G. Perumal Exploring the impact of laser surface oxidation parameters on surface chemistry and corrosion behaviour of AISI 316L stainless steel, *Applied Surface Science Advances*, Volume 22 100622, 2024, https://doi.org/10.1016/j.apsadv.2024.100622

[20] F. Brihmat-Hamadi, E. Amara et al. Surface laser marking optimization using an experimental design approach, *Applied Physics A*, 123, 230, 2017, https://doi.org/10.1007/s00339-017-0802-z

[21] K. Zhang, T. Liu Influence of laser parameters on the surface morphology of slurry-based Al2O3 parts produced through selective laser melting, *Rapid Prototyping Journal*, 24(3):00-00, 2018, DOI: https://doi.org/10.1108/RPJ-12-2016-0201

[22] H. Liu, W. Lin; M. Hong Surface coloring by laser irradiation of solid substrates, *APL Photonics*, 4 051101, 2019, https://doi.org/10.1063/1.5089778

[23] M. Pandey, B. Doloi, Experimental investigation into fibre laser marking on stainless steel 304, *Advances in Materials and Processing Technologies*, 9(4):1-14, 2022, DOI: https://doi.org/10.1080/2374068X.2022.2081302

[24] N. Angelov, L. Lazov et al., Influence of the Overlap Coefficient on the Contrast in Laser Marking of C110W Steel, *Environment. Technology. Resources. Rezekne, Latvia, Proceedings of the 13th International Scientific and Practical Conference*. Volume 3, 15-19, 2021, https://doi.org/10.17770/ETR2021VOL3.6599